Enhancement of Microgrid Operation by Considering the Cascaded Impact of Communication Delay on System Stability and Power Management

Navid Aghanoori, *Student Member*, *IEEE,* Mohammad A.S. Masoum, *Senior Member, IEEE*, A. Abu-Siada, *Senior Member, IEEE,* Syed Islam, *Fellow, IEEE*

Abstract- **Power management, system stability and communication structure are three key aspects of microgrids (MGs) that have been explored in many research studies. However, the cascaded effect of communication structure on system stability followed by the impact of stability on the power management has not been fully explored in the literature yet and needs more attention. This paper not only explores this cascaded impact, but also provides a comprehensive platform to optimally consider three layers of MG design and operation from this perspective. For generation cost minimization and stability assessment, the proposed platform uses an adaptive particle swarm optimization (PSO) while a new class of data exchange scheme based on IEC 61850 protocol is proposed to reduce the communication time delays among the inverters of distributed generations and the MG control center. This paper also considers the system stability using small-signal model of a MG in a real-time manner as an embedded function in the PSO. In this context investigations have been conducted by modeling an isolated MG with solar farm, fuel cell generator and micro-turbine in MATLAB Simulink. Detailed simulation results indicate the proposed power and stability management method effectively reduces the MG generation cost through maximizing the utilization of the available renewable generations while considering system stability.**

Index Terms- **Microgrid, renewable energy, power management, stability, IEC 61850, GOOSE messaging.**

NOMENCLATURE

A_{MG-dr}, A_{MG-sh}	System Matrix of MG with Droop Control and Power Sharing
α_{DGi}	Power Sharing Reference for DG Inverter Unit i [pu]
CB	Circuit Breaker
CPSO	Co-evolutionary Particle Swarm Optimization (PSO)
C_{MG}, $C_{solar}(t)$, $C_{MT}(t), C_{FC}(t)$	Costs of MG, Solar Farm, Micro-turbine and Fuel Cell at Time t [$]
DG; DCS	Distributed Generator; Distributed Control System
GOOSE	Generic Object Oriented Substation Event
IED	Intelligent Electronic Device
K_{P-dr}^i, K_{Q-dr}^i	Proportional Gain for Active and Reactive Power Droop Control of DG Unit i
LC_{solar}, LC_{MT}, LC_{FC}, LC_{DGi}	Levelized Costs for Solar Farm, Micro-turbine, Fuel Cell and DG Unit i [$/kWh]
LN; MG	Logical Node; Microgrid
MMXU	IEC 61850 Measurement Unit Logical Node Name
N	Number of Nodes
NTP	Network Time Protocol
$p \in P, t \in T$	"places" and "transitions" in Petri Net
PN; PLC	Petri Net; Programmable Logic Controller
$P_{load}(t)$, $P_{DGi}(t)$	Total Power Demand of Loads and DG Unit i at Time t [W]
P_{DGi}^{min}, P_{DGi}^{max}	Minimum and Maximum Power Demand of DG Unit i [W]
P_{solar}, P_{MT}, P_{FC}	Power Reference Signals for Solar Farm, Micro-turbine and Fuel Cell [W]
SCADA; SV	Supervisory Control and Data Acquisition; Sampled Value
TCP/IP	Transmission Control Protocol/Internet Protocol
TCTR, TVTR	IEC61850 Current and Voltage Transformer Logical Node Name
τ	Communication Time Delay between MG Inverters and Control Centre [milliseconds]
v_{min}^i, v_{max}^i	Minimum and Maximum Voltage Limits [V]
$\omega_{min}^i, \omega_{max}^i$	Minimum and Maximum Frequency Limits [Hz]
X	States Vector
λ	Eigenvalues Vector of MG

I. INTRODUCTION

With the day-by-day increase of electricity demand, new strategies for power generation, transmission, distribution and management have been developed by utilities and industries. Microgrids (MGs) with renewable distributed generations (DGs) are powerful tools with significant effect in reducing central dispatch and dependency on the main grid particularly during network fault events. MG has numerous advantages including supplying local loads with the available local renewable resources while minimizing the utilization of conventional generations with less energy waste. MG can operate in network-connected and islanded modes using AC, DC or hybrid AC/DC power flow depending on the nature of the network design [1-3]. MG relies on renewable DGs to reduce the overall cost, energy waste and CO_2 emission. However, maximizing the utilization of DGs requires sophisticated control and fast communication technologies to achieve optimal power management with stable operating conditions. For example, frequency control has been one of the biggest problems in the State of South Australia. The blackout in the year 2017 in South Australia has been reported mainly due to sudden and significant deficit of power supply which resulted in frequency collapse that was much quicker than the response of the under-frequency load shedding control scheme [4]. This proves the fact that fast control methods and communication infrastructure are not only essential for power system protection but are also required for control purposes. The communication delays can be either from the type of the selected protocol, the hardware or the network layout chosen by the design engineer. It can also be caused by other reasons such as network traffic, faulty component, wrong firmware configurations, gateways or firewalls. While there is much research on real-time operation, control, decision making and stability of MGs [3, 5-16], none of the existing research directly addresses the issues, impacts and solutions associated with power references fluctuations and system time delays. For instance, reference [3] investigates the stability of the MG based on eigenvalue analysis assuming wind

N. Aghanoori and A. Abu-Siada are with the Department of Electrical and Computer Engineering, Curtin University, Perth, WA, Australia, E-mails: navid.aghanoori@postgrad.curtin.edu.au , a.abusiada@curtin.edu.au
M.A.S. Masoum is with the Department of Engineering, Utah Valley University, Orem, UT 84058 USA, E-mail (m.masoum@ieee.org)

Syed Islam is with the School of Science Engineering and Information Technology at Federation University, Ballarat, VIC 3350, Australia, E-mail: s.islam@federation.edu.au

speed fluctuations; however, the communication model and real-life time related constraints are not considered in this study. An energy storage system is proposed to damp the power oscillation caused by wind speed variations using small signal model analysis in [5] and reference [6] presents a DC MG stability model using small signal approximation and eigenvalue analysis without considering communication time delay in the droop control model. Reference [11] proposes a multiple time scale centralized hierarchical frequency stability control method for MV isolated MG, but it only illustrates the emergence of the fast communication in a limited frequency range. Reference [12] focuses on GOOSE messaging for protection purposes; however, it does not show details of the protocol such as its location within the control system infrastructure as well as the data class model structure.

Reference [13] presents a decentralized control architecture with continuous real-time decision-making considering system stability; however, the power references in the proposed controller are assumed to be constant which is not the case in real operation. The inverter-based MG model introduced in [5] and [13] is used in this paper. In [14] a virtual droop control is proposed to operate the MG under constant frequency and voltage operating conditions. The proposed droop control uses TCP/IP Modbus protocol to establish the communication between the natural gas generator and PLC; however, system time delay is not considered in the control system. In [3, 7-10] stability analyses of different MGs are investigated using small-signal models, but the communication time delay is ignored in the proposed centralized and decentralized power control schemes. Reference [15] investigates the time delay effect on power system stability in a centralized model while authors of [16] have explored the stability of a decentralized inverter control through wireless communications in a MG. Their findings indicate that increasing the time delay in a decentralized MG can move the eigenvalues of the system state space model from left to the right half of the complex s-plane indicating system instability. To maintain system stability a constant power sharing coefficient is proposed. However, the power references continuously change in real applications which if not considered, can lead to system instability.

References [31, 32] discuss optimal power management of MGs without the consideration of stability and communication time delay. While reference [33] considers system stability in the proposed power management, communication time delay is not considered in the investigation.

References [34, 35] consider the impact of time delay on the MG stability without considering the effects of stability on achieving optimal power management. These two references adopt different approaches for considering the time delay however, no technique is presented to mitigate this delay.

The above discussion shows there are many research efforts in which power management is solely considered and improved using various proposed methodologies. There is also numerous research work that cover the stability of MGs in which some consider the impact of communication delay to some extent but to the best of authors' knowledge, there has been no research or power management platform so far that simultaneously considers the following three important aspects of MGs:

- Investigate the cascaded impact of time delay on MG stability and the corresponding impacts on optimal power management.
- Propose a technique to minimize this cascaded impact by considering it in the cost objective function.
- Recommend a practical solution to reduce the impact of communication time delay between the MG control elements using IEC 61850. This work was initiated by the authors of this paper in [36] and was applied on a grid-connected wind farm in Australian grid for the purpose of voltage control improvement of remote utility-size renewable plants. In this paper, more comprehensive structure of this data class model is presented as a modular MG communication platform.

With simultaneous consideration of the above three aspects, the MG power management will be able to provide a proper control for the MG power demand with cost optimization at no risk on system stability. Additionally, the proposed data class model of IEC 61850 will allow all inverters from different vendors to interoperably communicate within few milliseconds without requiring any media conversion. This will also reduce the potential engineering hours and cost in relation to integration purpose. Table 1 presents a brief summary to the platforms proposed in the existing literatures and the research gap that this paper is covering.

In summary, this paper proposes a new centralized adaptive scheme for real-time power management and stability control of a MG based on the concept of power sharing presented in [16]. In this centralized adaptive scheme inverter reference signals are continuously updated at the MG control center using an adaptive Petri particle swarm optimization (PSO) and are transmitted to the DGs using a new data exchange model based on the IEC 61850 GOOSE messaging protocol. An isolated MG as shown in Fig. 1 with solar farm, fuel cell generator and micro-generator is simulated to check the performance of the proposed approach and investigate its sensitivity to time delays experienced in MGs with PLC/SCADA based control systems and conventional communication protocols.

TABLE I: Existing relevant studies versus the proposed platform of this paper

Reference Number	A: Optimal Power Management of MG	B: MG Stability	Impacts of "B" on "A"	C: Time Delay Impact on B	Cascaded Impacts of "A", "B" and "C"	Improvement Solution on:
[3,6-11]	✘	✔	✘	✘	✘	B
[13,31-32]	✔	✘	✘	✘	✘	A
[14]	✔	✔	✔	✘	✘	A, B
[15]	✘	✔	✘	✔	✘	B
[16,21]	✘	✔	✘	✔	✘	B, C
[17]	✘	✔	✘	✘	✘	B
[33]	✔	✔	✔	✘	✘	A, B
[34-35]	✘	✔	✘	✔	✘	B
This paper	✔	✔	✔	✔	✔	A, B, C

II. MG State Space Modelling Considering Time Delay

A MG can operate in islanded or grid-connected modes [16]. The frequency and power control of an islanded MG is more complicated due to the absence of grid that masters the frequency. This paper considers an isolated MG as shown in Fig. 1 that includes n units of DGs, H loads, L feeders and a centralized control center platform communicating with the inverters. Each DG is connected to a feeder through an inverter which contributes to the MG power management based on the reference signal generated by the proposed real-time control scheme. With the MG modular structure, the MG electrical model can be formulated and solved using state-space representation. The loads are also considered to be modular and can be either local or network utility loads that are fed by the MG. This paper treats all the loads as local MG loads.

A. General Observation on a State-space Model with Delay

This section illustrates how the location of eigenvalues changes due to a system time delay (T) using the general state-space representation of a linear-time invariant system as per the equation below.

$$\dot{x} = Ax(t-T) + Bu(t-T)$$
$$y = Cx(t-T) + Du(t-T) \qquad (1)$$

where A is the system dynamic matrix, B is the input matrix, C is the output matrix, D is the feedthrough matrix (assumed to be zero in the below analysis for simplicity), u is the input signal, y is the output of the system and x is the state variable of the system.

The system transfer function can be obtained from (1) using Laplace transform as below:

$$\frac{Y(s)}{U(s)} = \frac{C\,B\,e^{-sT}}{s - A\,e^{-sT}} \qquad (2)$$

Using all-pole approximation, the exponential function in (2) can be approximated as [37]:

$$e^{-sT} = \frac{1}{e^{sT}} = \frac{1}{1 + \frac{Ts}{1!} + \frac{(Ts)^2}{2!} + \frac{(Ts)^3}{3!} + \cdots} \cong \frac{1}{Ts+1} \qquad (3)$$

It is worth noting that all-pole approximation method is selected over Pade' approximation as it does not add a new zero to the system as per Pade' method and has less overshoot and adjusting time [37]. From (2) and (3), system transfer function can be written as:

$$\frac{Y(s)}{U(s)} = \frac{C\,B}{Ts^2 + s - A} \qquad (4)$$

The eigenvalues of the system are obtained from the characteristic equation of (4):

$$s^2 + \frac{1}{T}s - \frac{A}{T} = 0 \qquad (5)$$

It can be seen from (5) that by increasing the time delay T, the roots of the equation move toward the right hand side of the complex s-plane and after a critical point (depending on A and T), the roots become positive resulting in unstable condition.

B. MG Control Layout

The proposed MG control model is based on the concept of power sharing. However instead of relying on decentralized scheme presented in [16-17], this paper uses a centralized adaptive controller that continuously generates optimal inverter reference signals and transmits them to the DGs using a new fast IEC 61850 GOOSE messaging protocol. The optimal inverter reference signals are calculated using Petri PSO considering both generation cost and stability assessment based on small-signal MG model through eigenvalue analysis.

Fig. 2 shows the block diagram of one inverter including connections to the centralized control center and the IEC 61850 bus. The voltage and current regulator loops are included in the local inverters while the power management and stability controller that generates the optimal inverter reference signals is implemented in the MG centralized control center. The frequency and voltage of each source are calculated and transmitted to the corresponding inverter. All voltage and current controllers are referenced to d-q reference frame and traditional droop control strategy is used to control the angular frequency and voltage.
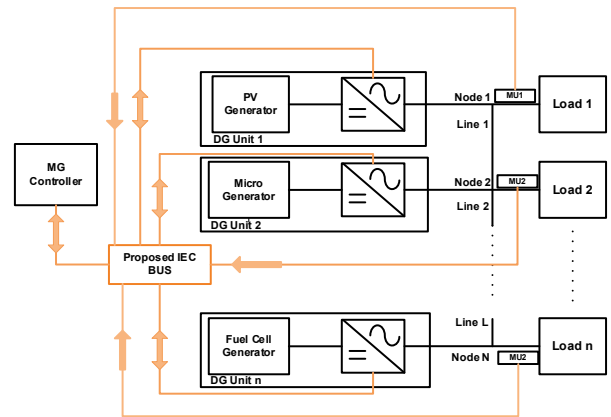

Fig. 1: The isolated MG under consideration with the addition of IEC 61850 Messaging (similar to the MG of [16-17] with PV, micro-turbine and fuel cell generators).
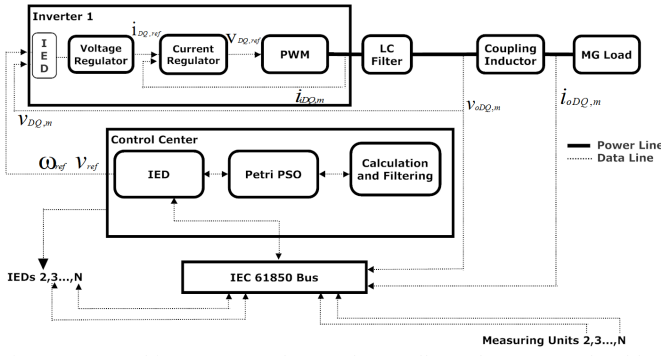
Fig. 2: Proposed inverter control, central controller and IEC 61850 bus block diagram.

Fig. 2 illustrates how data collection and updated reference signals are communicated within the MG control model. The p-q components of the voltage and current of each inverter are first measured and transferred to the main controller. Then, an adaptive control scheme is used to calculate the new power references and transmit them back to the inverters. It is to be noted that two voltage and current controllers are located locally in the inverters; however, the proposed power and stability management approach is implemented in the main centralized MG controller. The MG stability equations considering communication time delays are presented in (6) through (12) below. Detailed discussions on the droop control and power sharing management are available in [16, 17, 21].

C. State-Space Models for DG Inverters

The state-space model of each inverter within the MG can be formulated as below [16]:

$$\Delta \dot{x} = A_1 \Delta x + B_1 M_1' \Delta v_{bDQ} \tag{6}$$

$$\Delta I_{oDQ} = C_1 \Delta x \tag{7}$$

$$\Delta \omega_{com} = C_{com} \Delta x \tag{8}$$

$$\Delta x = \left[\Delta \delta^{(g)} \, \Delta P^{(g)} \Delta Q^{(g)} \Delta S_Q^{(g)} \Delta S_{V,D}^{(g)} \Delta S_{V,Q}^{(g)} \Delta S_{I,Q}^{(g)} \Delta S_{I,Q}^{(g)} \right. \tag{9}$$
$$\left. \Delta i_{iD}^{(g)} \, \Delta i_{iQ}^{(g)} \, \Delta v_{oD}^{(g)} \, \Delta v_{oQ}^{(g)} \, \Delta i_{oD}^{(g)} \, \Delta i_{oQ}^{(g)} \right].$$

where x represents the 14 elements vector containing states of the inverters voltage and current regulators, coupling inductance and LCL filter.

D. State Space Model for the MG Considering Power Sharing and Communication Time Delay

The conventional small-signal model of a MG without considering time delays is based on the small-signal models of individual inverters as below [16-17]:

$$\begin{bmatrix} \Delta \dot{x} \\ \Delta i_{2DQ} \\ \Delta i_{3DQ} \end{bmatrix} = A_{MG} \begin{bmatrix} \Delta x \\ \Delta i_{2DQ} \\ \Delta i_{3DQ} \end{bmatrix} \tag{10}$$

In this paper, a time delay τ between the measurement and control elements is considered which is mainly due to the communication delay between the voltage and/or current measurement units, plant controller and the inverters. As such, (5) is modified to:

$$\begin{bmatrix} \Delta \dot{x} \\ \Delta i_{2DQ} \\ \Delta i_{3DQ} \end{bmatrix} = A_{MG-dr} \begin{bmatrix} \Delta x \\ \Delta i_{2DQ} \\ \Delta i_{3DQ} \end{bmatrix} + A_{MG-sh} \begin{bmatrix} \Delta x(t-\tau) \\ \Delta i_{2DQ}(t-\tau) \\ \Delta i_{3DQ}(t-\tau) \end{bmatrix} \tag{11}$$

where A_{MG-dr} and A_{MG-sh} include the state-space models of all individual inverters as well as the architecture of the MG in

state-space representation. These matrices are fairly large and their detailed formulations are documented in the appendix A [16].

E. Effects of Power Reference Upgrading

The inclusion of the communication time delays in the DG inverter reference signals impacts the overall stability of the MG by introducing additional variable τ in the dynamic equations of the state-space model. This variable may change the determinant roots of the dynamic matrix corresponding to the eigenvalues [16]:

$$\Omega(\lambda, \tau) = \lambda I_0 - A_{MG-dr} - A_{MG-sh} e^{-\lambda \tau} \tag{12}$$

In building matrices $A_{grid-dr}$ and A_{grid_sh} (Eqs. 10-12), α variables are defined to represent the desired levels of DG active and reactive power sharing [16]. α for DG_i is calculated from:

$$\alpha_i = P_{DGi}/P_{load}. \tag{13}$$

Since the total amount of power contributed by all DGs within the MG must be equal to the total demanded power, thus [16]:

$$\sum_1^n \alpha_{DGi} = 1. \tag{14}$$

The α values for DG inverters are included in the MG dynamic matrices in the small-signal state-space model [16, 17, 21].

The zeros of (7) provide the MG eigenvalues (λ) that ultimately determine system stability. Therefore, it is important to monitor the impacts of α_{DGi} values on the stability of the MG while continuously updating the inverter reference signals for generation cost minimization (Eq. 16). To avoid instable operating conditions, the proposed adaptive Petri PSO assesses the stability of the MG (Eq. 12) before transmitting the power sharing references to the inverters. Using fast data exchange model based on the IEC 61850 GOOSE messaging and SV will reduce the time delay τ and inherently prevents MG unstable operating conditions due to communication delay. Detailed equations of each inverter are discussed in [16, 17].

Therefore, as the α values, communication time delay and other frequency and voltage references exist in the state-space dynamic matrices, they can impact the stability and assuming all these parameters constant impacts the stability accuracy. As the focus of this paper is on the communication time delay, and α values, only the impact of these factors are shown for the stability in the form of eigenvalue location on the s-plan in figures 11 and figure 12 and table III.

III. PROPOSED REAL-TIME POWER MANAGEMENT AND STABILITY CONTROL SCHEME FOR MG

A. Petri PSO

PN is a graphical tool that visualizes the real-time status of a system. It can dynamically illustrate the system status utilizing four main elements including "places", "transitions", "tokens" and "arcs" that are denoted by $p \in P$, $t \in T$, red ball and arrows, respectively [19]. For example, when the system condition changes from the ith status to the $(i+1)^{th}$ status then the transition fires and token goes from place p_i to place p_{i+1}. Therefore, due to its simplicity and compatibility with dynamic changes, PN is a suitable graphical tool for supervisory, management and control of stochastic systems [19, 20]. In this paper, PN is proposed to perform real-time power management of a MG for seamless stability control while a CPSO algorithm [22] is used

to embark on cost optimization.

Most conventional MG optimization strategies are intended to perform cost minimizations without considering the system stability [23-26]. The proposed Petri PSO includes a link between the cost function and stability of the MG in PSO mathematical model to move away from solution regions with poor MG stability conditions. Therefore, the Petri PSO is intended to minimize the cost of inverter based MGs while the stability of the system is also monitored. This scheme includes two layers of control and monitoring:

- *Top Control Layer-* PN is mounted on this layer of the process to indicate overall layer and status of the system.
- *Lower Control Layer-* This layer is initiated in one of the places in PN and includes the CPSO with an objective cost minimization function (Eq. 16) while three constraints are used for demanded load and MG stability (Eqs. 17-23).

PN is selected to be the top layer controller since it is easy to impediment in the plant controllers such as PLC, SCADA and DCS. Moreover, PN is modular and understandable for any level of expertise and can perform many types of optimization, logic, calculation and complicated theory.

In the proposed PN (Fig. 3), p_1 to p_7 are the system statuses that can be found in (Eqs. 12, 15) while t_1 to t_8 are the transitions stated in (8). Once each transition condition is met at p_n, transition fires and shifts the system into the next stage (e.g., stage p_{n+1}). Each place then generates the corresponding command which may satisfy the next transition. In Fig. 3, the two red tokens show the present stage of the MG. The places ($\in P$) of the proposed PN are found in Table II. Fig. 3a shows the proposed Peri PSO implemented in the HIPS PN simulator. A red token is placed in p_1 and two adjacent transitions are highlighted in blue color. This status of PN indicates that the control process is starting while two transitions conditions are being considered. Fig. 3b indicates that: i) the start-up process has been finished, ii) as the inverters are healthy, the system is at p_2 which means CPSO is initiated in order to find the acceptable results. The rest of the process will continue with red token representing system status at each time [19, 20].
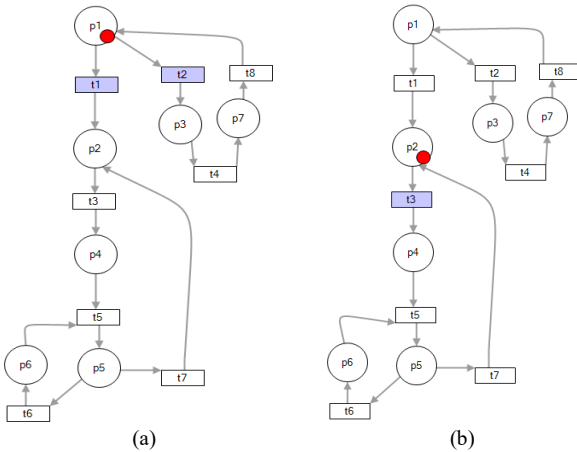

Fig. 3: Proposed MG Petri Net simulated in HIPS software with the system status; (a) at place 1, (b) at place 2.

TABLE II: PETRI NET CONFIGURATION ELEMENTS

Symbol	Definition
p_1	Starting the process and turning the inverter on
p_2, p_3, p_4	Running PSO, Resetting the fault, Sending references
p_5	Reading network data and comparing the cost
p_6	Keeping the references unchanged
p_7	Informing operator or restarting the device
t_1, t_2	Inverters are healthy, Inverters are not healthy
t_3, t_4	Communication is okay, Inverters are still faulty
t_5	Power measured values and time delay are received
t_6	Cost is within ±5% of optimal references
t_7, t_8	Cost is not within ±5%, Alarm is acknowledged

B. Petri PSO Cost Objective Function

In Fig. 3(b), the proposed Petri PSO algorithm is in place p_2 and will continuously generate the optimal inverter reference signals. The objective function of PSO is to minimize the overall MG generation cost. This is done using CPSO which is a co-evolutionary version of PSO [22] in order to generate the optimal DG inverter power sharing references (α_{DGi}). The objective function and constraints are the generation cost (Eq. 16) and the stability of the MG (Eqs. 17-20), respectively.

The selected MG cost objective function is [16]:

$$Min\ C_{MG}(t) = \sum_i^n C_{DGi}(t) = \sum_{i=1}^n LC_{DGi}P_{DGi}(t) \qquad (15)$$

where LC_{DGi} is the levelized cost of DG unit i in \$/kWh. For the MG under consideration with three generation sources, the cost function would be:

$$Min\ C_{MG}(t) = C_{solar}(t) + C_{MT}(t) + C_{FC}$$
$$= LC_{solar}P_{solar}(t) + LC_{MT}P_{MT}(t) + LC_{FC}P_{FC} \qquad (16)$$

where the selected levelized costs are LC_{solar}= 0 \$/kWh, $LC_{MT=}$ 0.06\$/kWh and LC_{FC}= 0.04\$/kWh [28]; however, these values depend on the MG type and location as well as thermal energy requirement that will affect the cost and contribution of FCs. In this paper it is assumed that the minimum power of fuel cells satisfies the minimum requirement of the thermal energy for the MG under consideration.

C. Petri PSO Constraints

There are three MG constraints considered in the minimization of the PSO objective function (Eq. 16):

1) *Power demand constraint-* requiring PSO particles to move towards solutions that satisfy the total load demand:

$$P_{load}(t) = \sum_{i=1}^n P_{DGi}(t) \qquad (17)$$
$$P_{DGi}^{min} < P_{DGi}(t) < P_{DGi}^{max} \qquad (18)$$

To avoid MG instability issues due to the variations in $P_{DGi}(t)$ caused by the stochastic nature of renewable DGs, the proposed CPSO algorithm must quickly and continuously compute the optimal values of α and use them to adjust the power sharing levels of each DG. This requires a seamless stability control and monitoring system with a fast communication scheme as proposed in Section IV; otherwise, fast dynamic variations such as rapid voltage sags or large scale spike may impact the control system either after the protection system has tripped or after some system equipment are damaged [29].

2) *Frequency and voltage constraint-* requiring MG frequency and voltage to be maintained within the acceptable limits of $[\omega_{min}^i, \omega_{max}^i]$ and $[v_{min}^i, v_{max}^i]$. The droop proportional coefficients for active and reactive power control of DG unit i are calculated as follows [16]:

$$K_{P-dr}^i = (\omega_{max}^i - \omega_{min}^i)/P_{max}^i \qquad (19)$$
$$K_{Q-dr}^i = (v_{max}^i - v_{min}^i)/Q_{max}^i \qquad (20)$$

3) *Stability constraint*- The third constraint is maintaining the stability of the MG [16]. The proposed CPSO algorithm continuously checks system stability using eigenvalue analysis for all MG frequency modes to ensure the variations in $P_{DGi}(t)$ and calculated α_{DGi} do not cause unstable conditions. This is done by selecting PSO populations that have particles with eigenvalues located in the left hand side of the complex s-plane (Eq. 12).

D. Adaptive Petri PSO

The adaptive nature of the proposed power management and stability control scheme is facilitated through real-time updating of DG inverter reference signals (α_{DGi}) based on Eqs. 13-16. This has the prominent advantage of maximizing the consumption of available renewable power based on real-time Petri PSO while also considering the MG stability. However, implementing this procedure with the conventional automation protocols used in PLC/SCADA system platform will introduce inherent time delays (Eqs. 11, 12) that may cause unstable operating conditions. To overcome this issue, a new and fast MG communication class model in IEC 61850 GOOSE messaging protocol is introduced in the next section.

Implementation of the stability analysis in Petri PSO are all in one single code of the MATLAB software platform. As the power management, Petri PSO and all associated programs are developed in C. Therefore, the entire code can be wrapped in any desired format to be used in other software or hardware platforms. For instance:

i. The code can be wrapped in Python or other languages to be opened in PSSE/PSCAD for the grid integration studies. This is very useful for gird-connected MGs which need to be checked against compliance requirement.

ii. The code also can be wrapped into any format that each controller programming language can be compiled in the hardware. This becomes the source code of the hardware once it is compiled to the desired language.

iii. Alternatively, a function block diagram can be made using the logic/source code. Then M2PLC can be used to compile the code to an executable file which can be downloaded to PLC.

IV. PROPOSED FAST DATA EXCHANGE COMMUNICATION SCHEME FOR MG BASED ON IEC 61850

The proposed real-time MG power management and stability control scheme (Section III) relies on adaptive Petri PSO of Eqs. 12-20 to continuously update α_{DGi} that requires a fast communication network. This section introduces a new class model of IEC 61850 GOOSE messaging to exchange information within the MG through IEC bus. Previously, this protocol has been mostly used for protection communication in substation automation.

A. IEC 61850 GOOSE Messaging Model and Infrastructure

The International Electrotechnical Commission (IEC) has published standard IEC 61850 for substation automation [30].

It contains details of communication architecture with the substation components such as circuit breakers, transformers and other protection devices. The main target of the IEC 61850 series is to bring interoperability between the intelligent electronic devices (IEDs) from a wide range of vendor supplies and substation functionalities. In particular, IEC 61850-7 published by the IEC technical committee 57 provides standards for power system control and associated communication, logical nodes, data classes and information exchange which are closely related to the subject of this paper. IED is one of the key physical components of the IEC 61850 substation automation model. IEDs are the logical devices containing Logical Nodes (LN) that represent the actual physical component in the field such as circuit breakers, which has the standard name of XCBR. The LN is determined in the configuration file which is being held by IED. Then in a lower level of configuration file, data and data-attribute are defined for each LN. Data can be the position of a CB with a wide range of data-attributes such as current position shown as stVal or ctlVal representing the current value measured by the corresponding current transformer (CT) of the line. Fig. 4 presents a related example from IEC 61850-7-1 published in 2003 [30].
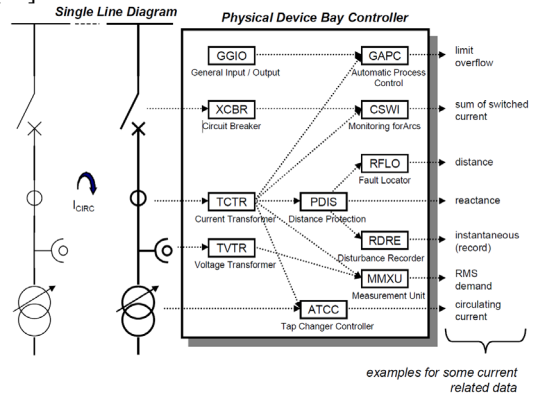

Fig. 4: Control and protection LNs combined in one physical device [30].

B. Proposed Class Model of IEC 61850 GOOSE Messaging and SV for a MG Inverter

Generic Object-Oriented Substation Event (GOOSE) messaging is one of the data models of IEC 61850 which provides fast communication between the IEC 61850 input data values of one IED to the output of other IEDs. The proposed scheme in this paper is presented with a new class model of GOOSE messaging to be used as the communication standard in a MG for faster communication between the control elements. The new communication model uses the existing measuring unit (Fig. 4) which relates to TCTR LN and TVTR LN. Each of these LNs transfers information to LN of measurement unit (MMXU). Additionally, assuming the main control center has IEDs and supports IEC 61850, only one IED is added into each inverter. Then the new customized data exchange with the purpose of power management, cost and stability control is implemented in the inverter IED and the controller IED. Fig. 5 shows the general model of GOOSE used in the proposed model to publish current and voltage values of each power line of the MG to the inverters and the main

controller IED. These values are then used in Petri PSO to generate new/updated DG inverter reference signals.
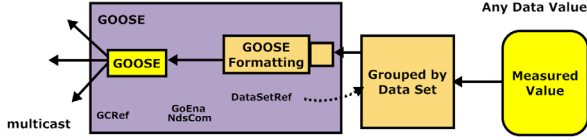

Fig. 5: Peer-to-peer data value publishing model (conceptual) [30].

On the other end of the peer-to-peer communication, a new class of model including the logical device, logical nodes, data and data-attributes needs to be generated to make the required information available for specific MG management and control purposes. The proposed class model of GOOSE messaging to achieve fast communication in inverter-based MG is presented in Fig. 6. It should be noted that the measurement section up to the multicast stage (Figs. 4, 5) are inherited from IEC 61850-7-2 and IEC 61850-7-3, however, in the configuration file current and voltage values are fed as analogue values into the GOOSE or SV data types. In this proposed model, the measurement unit is the publisher of the information while the main controller and the inverter's IEDs are publisher and subscriber of information, respectively.
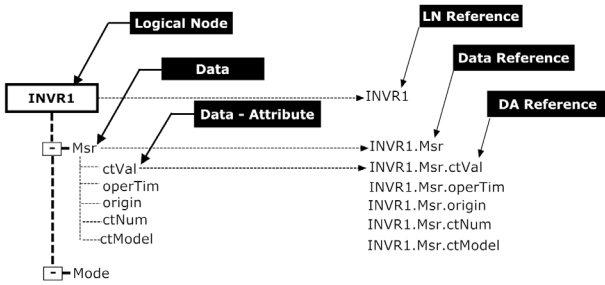

Fig. 6: MG inverter and controller information proposed structure illustrated as tree for the instance of current value measured by a CT shown in Fig. 4. [36]

Fig. 6 shows an example of the information exchange structure in a logical device such as MG inverter IED. This instance shows the layers of information structure in a tree format for the current value received from IEC 61850 measuring unit and TCTR logical node in physical device of bay controller (shown in Fig. 4). A logical node is created to represent inverter No. 1 of the line and since the information is categorized as measured data, the name "Msr" is assigned to the data. Msr data needs to have some sub data-attributes to provide clear physical meanings such as what type of device is used for generating the value, what is the operation time, what is the source of data ID, how many CTs are involved and what is the model of measurement. These features are considered as data-attributed references and denoted as ctVal, operTim, origin, ctNum and ctModel, respectively. According to IEC 61850, all data-attributes are known as different extensions of the same node when they are used in the configuration file. This guarantees the interoperability of standard for the proposed application of IEC 61850 GOOSE messaging and SV such that INVR1.Msr.ctVal is recognized in any IED which supports the IEC 61850 standard as "Measured current value of the corresponding power line of Inverter No.1". Figure 5 indicates the general scheme of multicasting a GOOSE message and the same concept is applied for SV but due to the lack of space only

GOOSE has been illustrated.

V. OVERALL COMPARISON BETWEEN EXISTING POWER MANAGEMENT ALGORITHMS AND PROPOSED PLATFORM

This section is presented to summarize the differences between existing power management algorithm and the proposed comprehensive platform which is facilitated with rea-time optimization and fast communication protocol.

The advantage of the proposed platform over the existing MG power management (Fig. 7a) are highlighted with yellow fonts in Fig. 7b. As can be seen in Fig. 7, the existing MG power management platforms:

- Do not consider the cascaded impact of time delay on stability and the impact of stability on MG operational cost,
- Don't have access to fast communication protocol for inverter control (few millisecond delay),
- Have not considered communication delays changes in real-time.
- Use constant ranges of frequency and voltage for their droop ratios and consequently, do not optimally update the frequency and voltage stability margins.
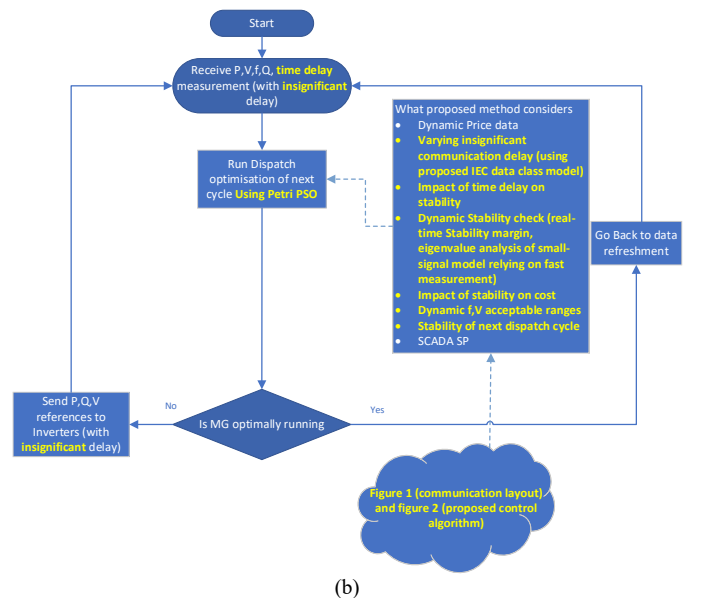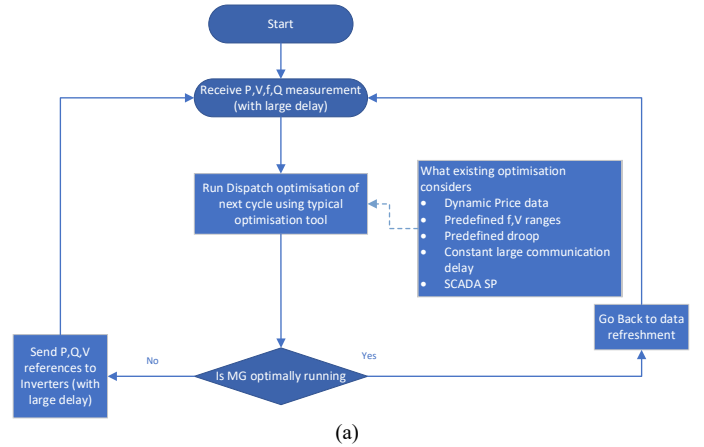

(a)

(b)

Fig. 7: a) The existing cost management method presented in several literatures [31,32], b) The proposed platform in this paper.

Based on the abovementioned points, the existing methods either situate the MG to a border line mode in which a small disturbance may result in system instability or operate in a very narrow operational margin in which renewable penetration and utilisation are not maximized.

The proposed power management of this paper not only considers and includes the abovementioned points, but also proposes a practical solution for each layer of management so that the proposed platform can provide a comperhensive solution for power management, cost control, communication control and high level SCADA monitoring. It should also be highlighted that the proposed platform presets a new data class model of IEC 61850 rather than relying on the existing protocols which are slow and/or non-interoperable.

VI. EXPERIMENTAL SETUP FOR MEASURING TIME DELAY OF THE PROPOSED IEC 61850 SV AND GOOSE DATA TYPE

A laboratory setup consisting of two industrial servers equipped with high speed full duplex network interface cards representing the IEC 61850 Server, Client and controller are used to experimentally demonstrate that the proposed data exchange protocol of Section IV.B can meet the maximum time delay requirement of 20 ms [16] for the MG of Fig. 1. Figure 8 shows the laboratory set up and screen shots from the Xelas Energy simulator platform which is used to simulate the IEC 61850 network and proposed data exchange monitoring. The two existing data types of IEC 61850 are utilized and the results are compared considering GOOSE and SV as the packet frames to share the information between IEDs. The two servers represent roles of IEC 61850 Server and Client (Fig.9, 10) while the digitalized data from an IED are transmitted to a controller and then calculated power sharing references (α_{DGi}; Eqs. 13, 14) are transmitted to each virtual IED. Both server and client have to be running throughout this test to be able to send and receive the packets. The Wireshark communication sniffer is only used to measure GOOSE and SV time delivery, respectively. As Wireshark is not capable of capturing all fast-transferred data, two data attributes were added to the data class named as "issued packet time" and "received packet time" with an associated packet label. When the packet is sent from the real-time IED, the "issued packet time" of the data attribute is filled by the clock of the IED. On the other hand, when the data attribute is delivered to other end of peer-to-peer communication the "received packet time" is recorded and sent back to the first IED. Wireshark which can be run on slow clock detects the packet with delays while the packet carries two recorded times considering the real time delay of the packet sent from one peer and delivered by the other. Using this method, the slow process of non-real-time software is ignored as it excludes the software processing time. This test bench was equipped with a GPS clock and the two simulators were synchronized to GPS via NTP. This made both peer's clock adequately matched in relation to accuracy of the time delay measurement.
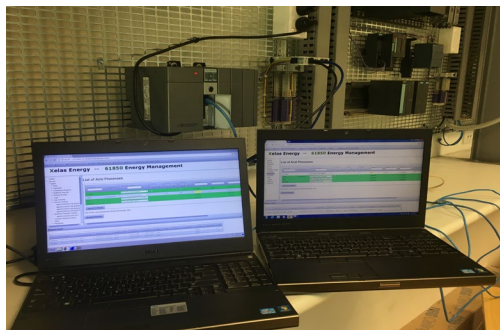

Fig. 8: Laboratory setup for communication test of the proposed new class of IEC 61850 GOOSE messaging.

As can be seen in Fig. 8, the client and server are running on IP address of 192.168.0.131 and 192.168.0.120 through the laboratory network. Fig. 9 indicates the delivery IEC packages on the client. As expected, the delivery time is changing from 2 to 4 ms for GOOSE while it is constant at 2 ms for SV. Both delivery times are configurable in the SCL file (Fig. 9). SV and GOOSE have their own advantages and limitations. The main diffrences are:

- SV perfromes sampling every 2 ms as set in SCL file and sends the value to the client, while GOOSE only takes the sample when an event occurs based on the maximum speed setting in the SCL file which eventually slows down to the minimum speed. These communication time delays exclude the overhead time of the windows.
- GOOSE message does not send an updated value unless the new event is triggered and it keeps repeating the same value till the next event happens whereas SV takes the sample and sends it through regardless.
- SV generates significantly more traffic in the network.

These experimental results show that the communication scheme of Section IV based on IEC 61850 with GOOSE and SV data types can meet the minimum time delay requirement of 20 ms for the MG of Fig. 1. This experiment was only implemented to show the capability of the proposed data class delivery and was only conducted between two IEDs.
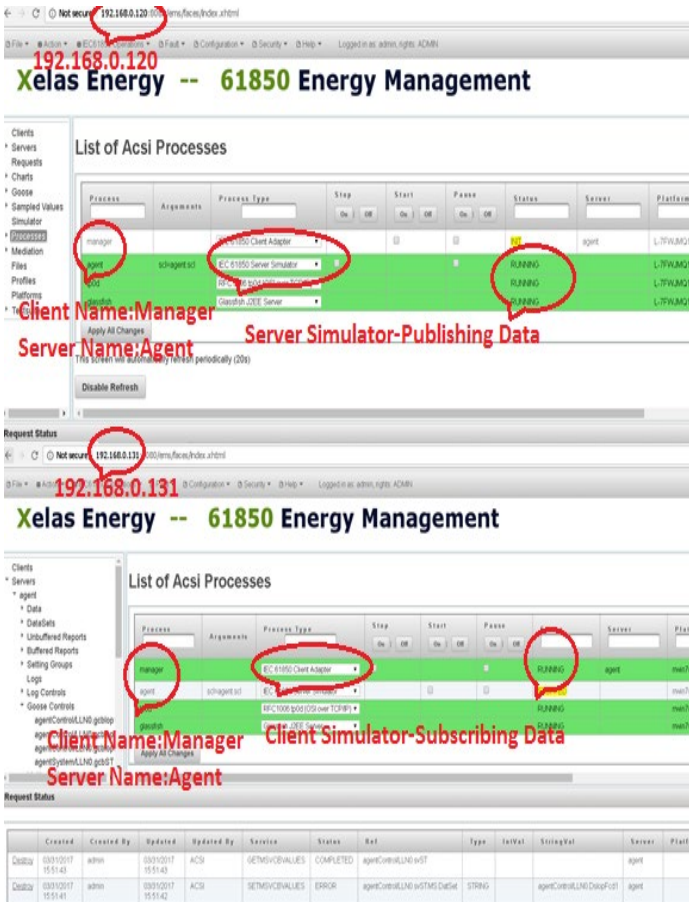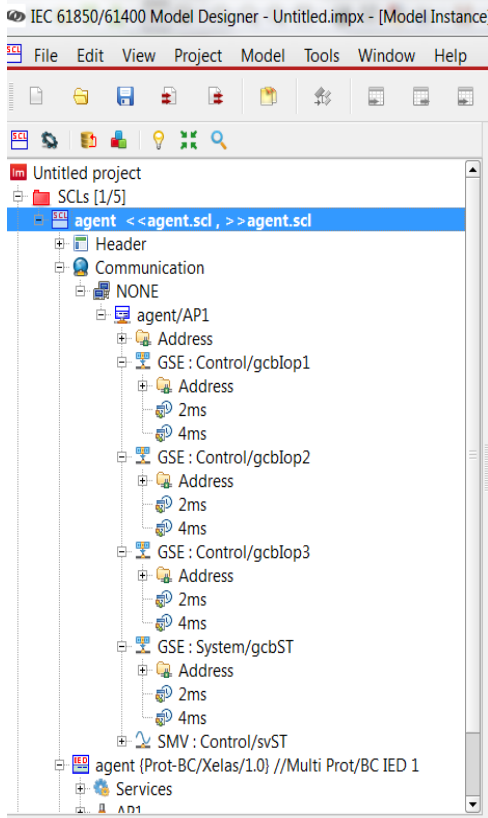
Fig. 9: IEC 61850 Server and Client Running on Xelas Energy Management Graphic User Interface (GUI).
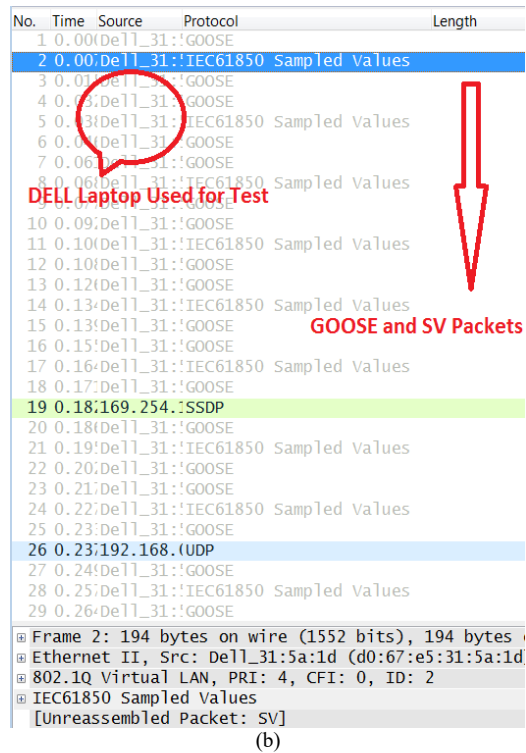

(a)

(b)

Fig. 10: (a) Server SCL file in model designer software package of Xelas Energy, (b) Wireshark IEC 61850 captured SVs at Client end.

VII. SIMULATION RESULT AND DISCUSSIONS

To evaluate the performance of the proposed centralized adaptive power management and stability control scheme and investigate its sensitivity to the MG communication time delays, MG of Fig. 1 is simulated using MATLAB Simulink and is subjected to different inverter power sharing references (α_{DGi}) and time delays as in the below case studies.

A. Case A: Impacts of Time Delay on MG Stability

The impacts of slow communication between the inverters and controllers on the MG stabilty are investigated by simulating the proposed centralized adaptive power management without considering CPSO constraint 3 (Section III.B). The calculated optimal cost (Eq. 16) is 0.026946 $/kWh regardless of the time delay while the power sharing references sent to the inverters are 0.7212, 0.2683 and 0.0105 pu for solar, fuel cell and micro turbine, respectively. Figure 11 presents simulation results for the MG of Fig. 1 including the locations of eigenvalues on the complex s-plane with the time delay slowly increasead from 1 to 30 ms with a step of 1 ms. To exclusively investigate the impacts of time delay, all eigenvalues are calculated using the same power sharing reference values. Regarding Fig. 11:

- Each branch of blue color stars represents the movement of an eigenvalue as τ is increased from 1 to 30 ms.
- Some of eigenvalues are moved from the left half side of the s- plane (stable region) towards the right half plane (instable region) as τ is slowly increasead. These modes are sensitive to time delays and can cause unstable operating conditions.
- There are some modes with eigenvalues being very close to the imaginary axis. These modes can cause steady state frequency and voltage fluctuations and may also make the

MG unstable in the event of small disturbance.

- There are also more eigenvalues positioned relatively far from the imaginary axis that are not shown in Fig.10 since they will not be moved to the right half plane and the system will remain stable in these modes with high stability and gain margins.

Based on the experimental results of Section V, the IEC 61850 GOOSE and SV provide fast communication such that the time delay for MG of Fig. 1 is less than 20 ms which will situate all eigenvalues in the left half side of the s-plane and hence ensures system stability.
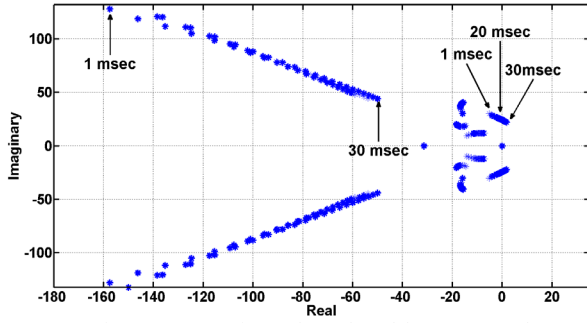

Fig. 11: Low frequency MG eigenvalues plotted for τ=1 ms and τ=30 ms.

B. Case B: Performance of MG with the Proposed Real-Time Power Management and Stability Control Scheme

The proposed real-time power management and stability control scheme of Section III is evaluated for the MG of Fig. 1 considering communication time delays of 5 and 15 ms (Table III). It is worth mentioning that both time delays are within the stable zone (Fig. 11) and achievable by the proposed IEC 61850 SV and GOOSE data exchange communication scheme. Figure 12 shows that the critical low frequency eigenvalues move towards the right half plane as the time delay changes from 5 to 15 ms.
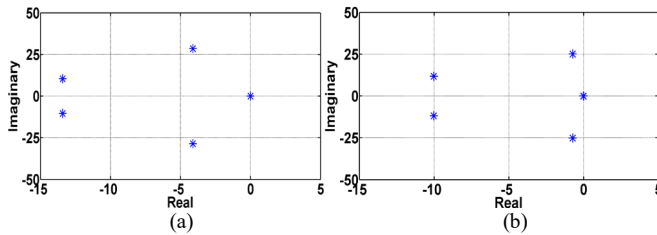

Fig. 12: Low frequency eigenvalues of MG for: (a) τ=5 ms, (b) τ=15 ms.

TABLE III: SUMMARY OF SIMULATION RESULTS

| Case | Stability Constraint | τ [ms] | α_{DGi} [pu] for | | | Cost [$/kWh] | Stable |
			P_{Solar}	P_{FC}	P_{MT}		
A1	Not Considered	τ>20	0.721	0.268	0.010	0.0269	No (Fig. 11)
A2	Not Considered	0<τ<19	0.721	0.268	0.010	0.0269	Yes (Fig. 11)
B1	Considered	τ=5	0.624	0.278	0.098	0.0366	Yes (Figs. 12a,13)
B2	Considered	τ=15	0.577	0.348	0.074	0.0418	Yes (Figs. 12b,14)

Table III intends to show and summarize the cascaded impact of time delay on the stability and impact of considering the stability on the power management cost of the MG in two sets of simulations:

- ✓ The first set includes scenarios A1 and A2. In case A1, MG is not stable if the time delay of control system is above 20 milliseconds. If the propose data class model of IEC 61850 is used (case A2), the time delay will be smaller than 20 ms which makes the exact operational scenario; however, for some other scenarios in which power sharing factor move as per cost optimization, the system will become unstable. It is worth noting that this paper, in section VI, has illustrated that the proposed protocol can provide communication delay smaller than 20 milliseconds.

- ✓ The second set of simulations compares scenarios B1 and B2 in which the time delay is below 20 millisecond and Petri PSO considers the stability constraint in the optimization algorithm to ensure only references are sent to the inverters that are no risk to instability of MG. Between these two simulations that both have access to relatively fast communication platform, the results show the MG with smaller communication time delay (faster communication protocol) has lower cost (B1). The reason for this cost saving is that the optimization algorithm of MG B1 can adjust the power sharing factor (α gains) more towards cheaper source of power relying on the faster communication protocol and its impact on locating the eigenvalues more away from right hand side of the s-plane. This practically means faster communication allows a better power sharing weighting factor which conclude with better cost and power management of MG.
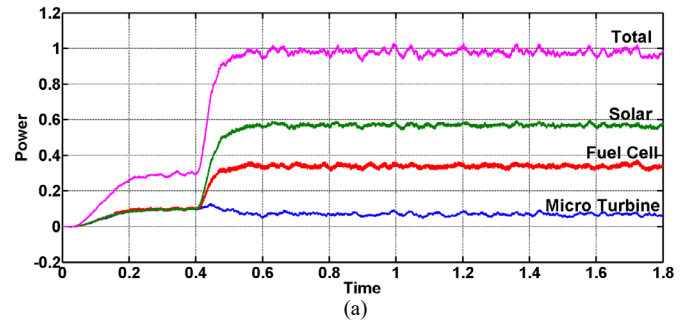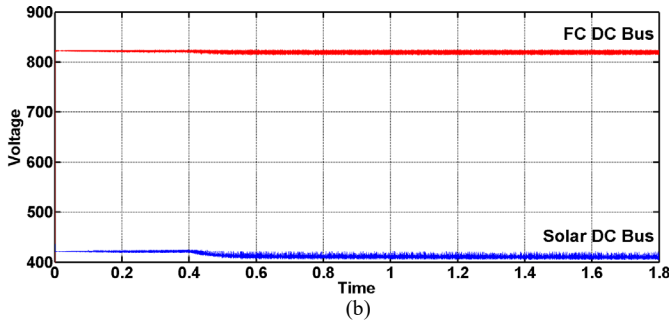
Fig. 13: (a) Power output from each inverter with τ=5 ms, (b) DC voltage of Solar and FC inverters with τ=5 ms.
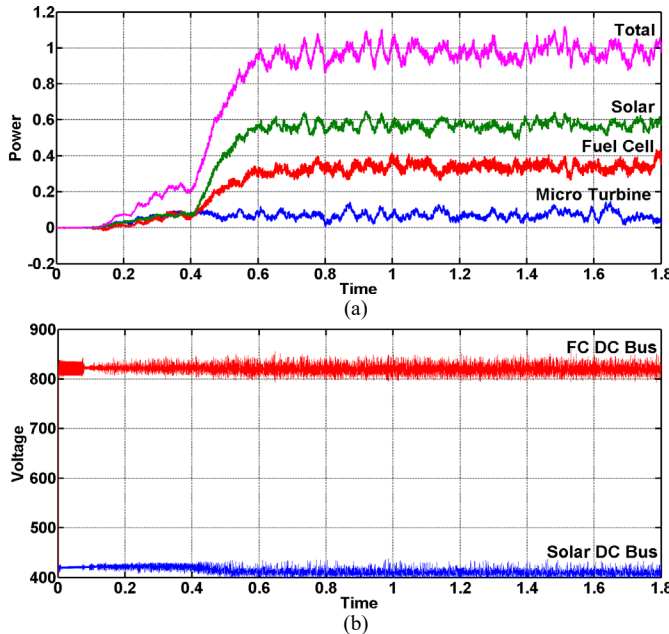

Fig. 14: (a) Power output from each inverter with τ=15 ms, (b) DC voltage of solar and FC inverters with τ=15 ms.

Figures 13 and 14 show the total and DG output power profiles, as well as the DC bus voltages with time delays of 5 and 15 ms, respectively. It is clearly seen that increasing the time delay even within the stable limit of 20 ms [16] will generate considerable fluctuations and oscillations in the output power and the DC voltage of each DG inverter. These fluctuations could significantly deteriorate the MG power quality. In some occasions, such fluctuations may also damage the equipment or cause incorrect protection tripping in the MG.

C. Comments on Selected Time Delay
The selected critical time delay of 20 ms for the case scenarios of the paper is from [16]. For the simulated microgrid, as shown in the appendix, small signal analysis is considered for generic time delay (as per Eq. 16) caused by communication between all the control elements. By adjusting the time delay it is observed in reference [16] and confirmed in Figure 11 of this paper that for such system and such control parameters, any communication delay larger than 20 ms causes the eigenvalues to move to the right hand side of the complex s-plane which means the system is unstable beyond this time delay. Therefore, the 20-ms time delay is used as the critical time delay for this system.

The time delay can vary for different reasons and there are also different ways of managing the instability caused by time delays. For instance, the controller gains can be tuned to shift the cross-over points of the bode plot for an unstable system to the area that has a phase margin of 0 to -180. However, by doing so we are lowering the bandwidth of the controller which limits the speed of the system response. This will result in a system which is less responsive to disturbances. Therefore, at the first place the designers need to reduce the time delay which provides a larger control margin to the system.

VIII. CONCLUSION

This paper firstly highlights the absence of an existing study that explores the cascaded impact of communication delay on the MG's stability and the effects of MG's stability on the power management cost. This paper then proposes a real-time power management platform to address these important aspects of MG's through the following contributions.

1- The proposed technology provides a fast communication platform to:
- Improve the stability of MGs.
- Facilitate the power management with real-time data for dynamic small-signal analysis.
- Enable various renewable sources to communicate in an interoperable manner with minimal integration cost and time delay.

2- The proposed technology takes into account the impact of MG stability on the cost of power management by:
- Ensuring the MG stability is not compromised for cost management.
- Facilitating high renewable energy penetration since the power management has access to real-time high-resolution data, constraint range of power system can dynamically change.

Simultaneous consideration of items 1 and 2 above, in a cascaded manner using Petri-PSO, can provide unique opportunities to increase penetrations and participations of renewable DGs in MGs.

Some further detailed conclusions of the simulation and experimental tests of the proposed platform can be drawn as below:
- The proposed real-time power management and stability control method can minimize the overall generation cost while considering MG stability conditions. The proposed method utilizes adaptive Petri PSO for real time calculation of DG power sharing references considering MG stability while the SV and GOOSE messaging of IEC 61850 substation protocol is used to reduce the communication time delays.
- In the MG's studied in this paper, increasing the time delay even within the stable limit of 20 ms will generate considerable fluctuations and oscillations in the output power and the DC voltage of each DG inverter.
- Based on experimental measurement, both data-exchange models based on SV and GOOSE messaging can provide acceptable time delays within the maximum limit of 20 ms. However, SV is a better data type to transfer information over IEC 61850 bus while GOOSE can achieve the same

result but requires event definitions.

- Conventional dispatching and communication methods with relatively large time delays without considering stability constraints can perform power management with slightly less generation cost but may situate the eigenvalues in the unstable side of the complex s-plane.

REFERENCES

[1] F. Nejabatkhah and Y. W. Li, "Overview of power management strategies of hybrid AC/DC microgrid," *IEEE Trans. on Power Electronics*, vol. 30, no. 12, pp. 7072-7089, 2015.

[2] L. Meng, T. Dragicevic, J. Roldán-Pérez, J. C. Vasquez and J. M. Guerrero, "Modeling and sensitivity study of consensus algorithm-based distributed hierarchical control for DC microgrids," *IEEE Trans. on Smart Grid*, vol. 7, no. 3, pp. 1504-1515, 2016.

[3] X. Tang, W. Deng and Z. Qi, "Investigation of the dynamic stability of microgrid," *IEEE Trans. on Power Systems*, vol. 29, no. 2, 2014.

[4] C. Uhlmann, "South Australia's storm caused Transmission Faults, But That's Not The Whole Story," ABC NEWS, NSW. [Online]. http://www.abc.net.au/news/2016-10-19/wind-power-loss-key-event-in-sa-blackout-report-finds/7947478.

[5] J. A. P. Lopes, C. L. Moreira, and A. G.Madureira, "Defining control strategies for microgrid ESS islanded operation," *IEEE Trans. Power Systems*, vol. 21, no. 2, pp. 916–924, 2006.

[6] S. Anand and B. G. Fernandes, "Reduced-order model and stability analysis of low-voltage DC microgrid," *IEEE Trans. on Industrial Electronics*, vol. 60, no. 11, pp. 5040-5049, 2013.

[7] X. Guo, Z. Lu, B. Wang, X. Sun, L. Wang and J. M. Guerrero, "Dynamic phasors-based modeling and stability analysis of droop-controlled inverters for microgrid applications," *IEEE Trans. on Smart Grid*, vol. 5, no. 6, pp. 2980-2987, 2014.

[8] A. Haddadi, B. Boulet, A. Yazdani and G. Joós, "A μ-based approach to small-signal stability analysis of an interconnected distributed energy resource unit and load," *IEEE Trans. on Power Delivery*, vol. 30, no. 4, pp. 1715-1726, 2015.

[9] R. Majumder, "Some Aspects of Stability in Microgrids," *IEEE Trans. on Power Systems*, vol. 28, no. 3, pp. 3243-3252, 2013.

[10] I. P. Nikolakakos, H. H. Zeineldin, M. S. El-Moursi and N. D. Hatziargyriou, "Stability evaluation of interconnected multi-inverter microgrids through critical clusters," *IEEE Trans. on Power Systems*, vol. 31, no. 4, pp. 3060-3072, 2016.

[11] Z. Zhao, P. Yang, J. M. Guerrero, Z. Xu and T. C. Green, "Multiple-time-scales hierarchical frequency stability control strategy of medium-voltage isolated microgrid," *IEEE Trans. on Power Electronics*, vol. 31, no. 8, pp. 5974-5991, 2016.

[12] Hongxia Wu, K. S. Tsakalis and G. T. Heydt, "Evaluation of time delay effects to wide-area power system stabilizer design," *IEEE Trans. on Power Systems*, vol. 19, no. 4, pp. 1935-1941, 2004.

[13] C. M. Colson and M. H. Nehrir, "Comprehensive real-time microgrid power management and control with distributed agents," *IEEE Trans.on Smart Grid*, vol. 4, no. 1, pp. 617-627, 2013.

[14] A. Solanki, A. Nasiri, V. Bhavaraju, Y. L. Familiant and Q. Fu, "A new framework for microgrid management: virtual droop control," *IEEE Trans. on Smart Grid*, vol. 7, no. 2, pp. 554-566, 2016.

[15] F. Milano and M. Anghel, "Impact of time delays on power system stability," *IEEE Trans. on Circuits and Systems I: Regular Papers*, vol. 59, no. 4, pp. 889-900, 2012.

[16] H. Liang, B. J. Choi, W. Zhuang and X. Shen, "Stability enhancement of decentralized inverter control through wireless communications in microgrids," *IEEE Trans. on Smart Grid*, vol. 4, no. 1, 2013.

[17] N. Pogaku, M. Prodanovic and T. C. Green, "Modeling, analysis and testing of autonomous operation of an inverter-based microgrid," *IEEE Trans. on Power Electronics*, vol. 22, no. 2, pp. 613-625, March 2007.

[18] T. Niknam, H. Z. Meymand, H. D. Mojarrad and J. Aghaei, "Multi-objective daily operation management of distribution network considering fuel cell power plants," *IET Renewable Power Generation*, vol. 5, no. 5, pp. 356-367, 2011.

[19] T. Murata, "Petri nets: Properties, analysis and applications," in *Proceedings of the IEEE*, vol. 77, no. 4, pp. 541-580, April 1989.

[20] X. Lu, M. Zhou, A. C. Ammari and J. Ji, "Hybrid Petri nets for modeling and analysis of microgrid systems," in *IEEE/CAA Journal of Automatica Sinica*, vol. 3, no. 4, pp. 349-356, Oct. 2016.

[21] C. Dou, M. Lv, T. Zhao, Y. Ji and H. Li, "Decentralised coordinated control of microgrid based on multi-agent system," in *IET Generation, Transmission & Distribution*, vol. 9, no. 16, pp. 2474-2484, 2015.

[22] Q. He, L. Wang and F. z. Huang, "Nonlinear constrained optimization by enhanced co-evolutionary PSO," *IEEE Congress on Evolutionary Computation*, Hong Kong, pp. 83-89, 2008.

[23] C. C. Thompson, P. E. Konstantinos Oikonomou, A. H. Etemadi and V. J. Sorger, "Optimization of data center battery storage investments for microgrid cost savings, emissions reduction, and reliability enhancement," *IEEE Trans.* on Industry Appli., vol. 52, no. 3, 2016.

[24] T. A. Nguyen and M. L. Crow, "Stochastic optimization of renewable-based microgrid operation incorporating battery operating cost," *IEEE Trans. on Power Systems*, vol. 31, no. 3, pp. 2289-2296, May 2016.

[25] C. Li, F. de Bosio, F. Chen, S. K. Chaudhary, J. C. Vasquez and J. M. Guerrero, "Economic dispatch for operating cost minimization under real-time pricing in droop-controlled DC microgrid," *IEEE Journal of Emerging and Selected Topics in Power Electronics*, vol. 5, no. 1, pp. 587-595, March 2017.

[26] M. Zachar and P. Daoutidis, "Microgrid/Macrogrid energy exchange: A novel market structure and stochastic scheduling," *IEEE Trans. on Smart Grid*, vol. 8, no. 1, pp. 178-189, Jan. 2017.

[27] M. Y. El-Sharkh, M. Tanrioven, A. Rahman and M. S. Alam, "A study of cost-optimized operation of a grid-parallel PEM fuel cell power plant," *IEEE Trans. on Power Systems*, vol. 21, no. 3, 2006.

[28] S. Chowdhury and M. Y. El-sharkh, "A reinforcement learning algorithm based technique for thermal energy management of a PEM fuel cell power plant," *2015 IEEE Industry Applications Society Annual Meeting*, Addison, TX, pp. 1-8, 2015.

[29] N. Aghanoori and M. A. S. Masoum, "Voltage sag compensation in renewable plant using hydro-pump storage," *2015 IEEE PES Asia-Pacific Power and Energy Engineering Conference (APPEEC)*, Brisbane, QLD, pp. 1-5, 2015.

[30] IEC for basic communication structure for substation and feeder equipment Principles and models, IEC 61850-7-1, 2003.

[31] B. Zhao *et al*., "Energy Management of Multiple Microgrids Based on a System of Systems Architecture," *IEEE Trans. on Power Systems*, vol. 33, no. 6, pp. 6410-6421, Nov. 2018.

[32] H. Mahmood and J. Jiang, "Decentralized Power Management of Multiple PV, Battery, and Droop Units in an Islanded Microgrid," *IEEE Trans on Smart Grid*, vol. 10, no. 2, pp. 1898-1906, March 2019.

[33] Z. Yi, W. Dong and A. H. Etemadi, "A Unified Control and Power Management Scheme for PV-Battery-Based Hybrid Microgrids for Both Grid-Connected and Islanded Modes," *IEEE Trans on Smart Grid*, vol. 9, no. 6, pp. 5975-5985, Nov. 2018.

[34] *H. Yan, X. Zhou, H. Zhang, F. Yang and Z. Wu, "A Novel Sliding Mode Estimation* for Microgrid Control With Communication Time Delays," *IEEE Trans on Smart Grid*, vol. 10, no. 2, pp. 1509-1520, March 2019.

[35] G. Lou, W. Gu, Y. Xu, W. Jin and X. Du, "Stability Robustness for Secondary Voltage Control in Autonomous Microgrids With Consideration of Communication Delays," *IEEE Transactions on Power Systems,* vol. 33, no. 4, pp. 4164-4178, July 2018.

[36] N. Aghanoori, M. A. S. Masoum, S. Islam, A. Abu-Siada and S. Nethery, "Improving voltage of remote connection using wind-solar farms equipped with new voltage control strategy based on virtual impedance monitoring enabled by IEC 61850 communication," *IET Generation, Transmission & Distribution*, vol. 13, no. 11, pp. 2199-2207, 2019.

[37] Lin Xueyan and Ye Zheng, "Comparison of time delay processing methods in control system," *2015 4th International Conference on Computer Science and Network Technology (ICCSNT)*, Harbin, 2015, pp. 1502-1505.

STATE SPACE MODEL OF DG INVERTERS [16, 17]

$$P^{inv} = v_{od}^{inv} i_{od}^{inv} + v_{oq}^{inv} i_{oq}^{inv} \tag{A.1}$$

$$q^{inv} = v_{od}^{inv} i_{oq}^{inv} - v_{oq}^{inv} i_{od}^{inv} \tag{A.2}$$

Controller outputs and the corresponding voltages are derived as below:

$$i_{R,id}^{inv} = K_{pv}(v_{R,od}^{inv} - v_{od}^{inv}) + K_{iv} \int (v_{R,od}^{inv} - v_{od}^{inv}) dt - \omega_0 C_f v_{oq}^{inv} + F i_{od}^{inv} \tag{A.3}$$

$$i_{R,iq}^{inv} = K_{pv}(v_{R,oq}^{inv} - v_{oq}^{inv}) + K_{iv} \int (v_{R,oq}^{inv} - v_{oq}^{inv}) dt + \omega_0 C_f v_{od}^{inv} + F i_{oq}^{inv} \tag{A.4}$$

$$v_{R,id}^{inv} = K_{pi}(i_{R,id}^{inv} - i_{id}^{inv}) + K_{ii} \int (i_{R,id}^{inv} - i_{id}^{inv}) dt - \omega_0 L_f i_{iq}^{inv} \tag{A.5}$$

$$v_{R,iq}^{inv} = K_{pi}(i_{R,iq}^{inv} - i_{iq}^{inv}) + K_{ii} \int (i_{R,iq}^{inv} - i_{iq}^{inv}) dt + \omega_0 L_f v_{oq}^{inv} \tag{A.6}$$

where K_{pv} and K_{iv} are the proportional and integral gains of the voltage controller and K_{pi} and K_{ii} are the proportional and integral coefficients of the current controller. C_f, L_f and F are the capacitance of the LC filter, inductance of the filter and feedforward gains, respectively.

The droop concept is brought to this MG model though the below equations:

$$\omega_{R\_dr}^{inv} = \omega_0 - K_{P-dr}^{inv} P^{inv} \tag{A.7}$$

$$v_{R\_dr}^{inv} = v_{0,od} - K_{Q\_dr}^{inv} Q^{inv} \tag{A.8}$$

$$v_{R-dr}^{inv} = 0 \tag{A.9}$$

where K_{P-dr}^{inv} and $K_{Q\_dr}^{inv}$ are the frequency and voltage gains within a specific range accepted by the system which MG is connected to.

The below equations reveal the response of the MG need for active and reactive power.

$$P_{tot} = \int_{inv=1}^{g} P^{inv} \tag{A.10}$$

$$Q_{tot} = \int_{inv=1}^{g} Q^{inv} \tag{A.11}$$

By substituting each MG's source (A.10) and (A.11) can be updated to:

$$\omega_R^{inv} = \omega_{R\_dr}^{inv} + K_{P-sh}^{inv}[\alpha_p^{inv} P_{tot} - P^{inv}] \tag{A.12}$$

$$v_{R\_od}^{inv} = v_{Rdr,od}^{inv} + K_{Q-sh}^{inv} \int \alpha_Q^{inv} Q_{tot} - Q^{inv} dt \tag{A.13}$$

$$v_{R-oq}^{inv} = 0 \tag{A.14}$$

where K_{P-sh}^{inv} and K_{Q-sh}^{inv} are the power sharing gains.

The updated formulas with consideration of time delays are derived as:

$$\omega_R^{inv} = \omega(t)_{R\_dr}^{inv} + K_{P-sh}^{inv}[\alpha_p^{inv} P(t - \tau)_{tot} - P(t - \tau)^{inv}] \tag{A.15}$$

$$v_{R\_od}^{inv} = v(t)_{Rdr,od}^{inv} + K_{Q-sh}^{inv} \int \alpha_Q^{inv} Q(t - \tau)_{tot} - Q(t - \tau)^{inv} dt \tag{A.16}$$

$$v_{R-oq}^{inv} = 0 \tag{A.17}$$

where $\omega(t)_{R\_dr}^{inv}$ and $v(t)_{Rdr,od}^{inv}$ are calculated by (A.1) and (A.2).

Similarly, the power controllers which incorporate the total value of active and reactive power of all the inverters and generation in the MG are given as:

$$\dot{\Delta\delta}^{inv} = \left[-K_{P_{dr}}^{inv} + K_{P_{sh}}^{inv}\alpha_P^{inv} - K_{P_{sh}}^{inv}\right]\Delta P^{inv}$$

$$+ \sum_{\substack{i=0 \\ i \neq g}}^{g}[K_{P\_sh}^{inv}\alpha_P^{inv}\Delta P^{inv}] - \Delta\omega_{com} \tag{A.18}$$

$$\dot{\Delta P}^{inv} = -\omega_c\Delta P^{inv} + \omega_c I_{od}^{inv}\Delta v_{od}^{inv}$$

$$+ \omega_c I_{oq}^{inv}v_{oq}^{inv} + \omega_c V_{od}^{inv}\Delta i_{od}^{inv} + \omega_c V_{oq}^{inv}i_{oq}^{inv} \tag{A.19}$$

$$\dot{\Delta Q}^{inv} = -\omega_c\Delta Q^{inv} + \omega_c I_{oq}^{inv}\Delta v_{od}^{inv} - \omega_c I_{od}^{inv}\Delta v_{oq}^{inv}$$

$$- \omega_c V_{oq}^{inv}\Delta i_{od}^{inv} + \omega_c V_{od}^{inv}\Delta i_{oq}^{inv} \tag{A.20}$$

The integrator state of the power controller elements is denoted as S_Q^{inv} and the state is summarised in the equation in (A.21) below.

$$\Delta\dot{S}^{inv} = \alpha_Q^{inv}\sum_{inv=1}^{g}\Delta Q^{inv} - \Delta Q^{inv} = \left[\alpha_Q^{inv} - 1\right]\Delta Q^{inv} + \alpha_Q^{inv}\sum_{\substack{inv=1 \\ inv \neq g}}^{g}\Delta Q^{inv} \tag{A.21}$$

Then the small signal output of the power controller can be written as:

$$\Delta v_{R\_dr}^{inv} = -K_{Q\_dr}^{inv}\Delta Q^{inv} + K_{Q\_sh}^{inv}\Delta S_Q^{inv} \tag{A.22}$$

$$v_{R-oq}^{inv} = 0 \tag{A.23}$$

Small signal of gth inverter within the MG is worked out as follows.

$$\Delta\omega_{com} = \Delta\omega_R^g \tag{A.24}$$

$$\Delta\omega_{com} = \left[-K_{P\_dr}^g + K_{P\_sh}^g\alpha_P^g - K_{P\_sh}^g\right]\Delta P^g + \sum_{\substack{i=1 \\ i \neq g}}^{G}[K_{P\_sh}^g\alpha_P^g\Delta P^i] \tag{A.25}$$

Taking these outputs into state-space model adds additional states of $\Delta S_{V,D}^{(g)}$ $\Delta S_{V,Q}^{(g)}$ $\Delta S_{I,Q}^{(g)}$ and $\Delta S_{I,Q}^{(g)}$.

More comprehensive explanations can be found in [16, 17].

The state-space model of each inverter within the MG is [16,17]:

$$\Delta\dot{x} = A_1\Delta x + B_1 M_1'\Delta v_{bDQ} \tag{A.26}$$

$$\Delta\dot{I}_{oDQ} = C_1\Delta x \tag{A.27}$$

$$\Delta\omega_{com} = C_{com}\Delta x \tag{A.28}$$

$$\Delta x = \left[\Delta\delta^{(g)}\ \Delta P^{(g)}\Delta Q^{(g)}\Delta S_Q^{(g)}\Delta S_{V,D}^{(g)}\ \Delta S_{V,Q}^{(g)}\ \Delta S_{I,Q}^{(g)}\ \Delta S_{I,Q}^{(g)}\right.$$

$$\left.\Delta i_{iD}^{(g)}\ \Delta i_{iQ}^{(g)}\ \Delta v_{oD}^{(g)}\ \Delta v_{oQ}^{(g)}\ \Delta i_{oD}^{(g)}\ \Delta i_{oQ}^{(g)}\right] \tag{A.29}$$

where x is a 14 - element vector containing states of the inverter's voltage and current regulators, coupling inductance and LCL filter. Therefore $\Delta\dot{x}$ are given by

$$\Delta\dot{x}^{inv} = A_1^{inv}\Delta x^{inv} + B_1^{inv}\Delta v_{b,DQ}^n + B_{com}^{inv}\Delta\omega_{com} +$$

$$\sum_{inv=1}^{g}B_{P,inv}^g\Delta x^{inv} + \sum_{inv=1}^{g}B_{Q,inv}^{inv}\Delta x^{inv} \tag{A.30}$$

where A_1^{inv} is given by the equations discussed above and shown in matrices of A_{11}^{inv} and A_{12}^{inv} below:

$$A_{11}^{inv} = \begin{bmatrix}
0 & -K_{p\_dr}^{inv} & 0 & 0 & 0 & 0 \\
0 & -\omega_c & 0 & 0 & 0 & 0 \\
0 & 0 & -\omega_c & 0 & 0 & 0 \\
0 & 0 & 0 & 0 & 0 & 0 \\
0 & 0 & -K_{Q\_dr}^{inv} & K_{Q\_sh}^{inv} & 0 & 0 \\
0 & 0 & 0 & 0 & 0 & 0 \\
0 & 0 & -K_{pv}K_{Q\_dr}^{inv} & K_{pv}K_{Q\_sh}^{inv} & K_{iv} & 0 \\
0 & 0 & 0 & 0 & 0 & K_{iv} \\
0 & -K_{P\_dr}^{inv}I_{iq}^{inv} & \dfrac{-K_{Q\_dr}^{inv}K_{pv}\,K_{pi}}{L_f} & \dfrac{K_{Q\_sh}^{inv}K_{pv}\,K_{pi}}{L_f} & \dfrac{K_{pv}\,K_{pi}}{L_f} & 0 \\
0 & K_{P\_dr}^{inv}I_{id}^{inv} & 0 & 0 & 0 & \dfrac{K_{pv}\,K_{pi}}{L_f} \\
0 & -K_{P\_dr}^{inv}V_{oq}^{inv} & 0 & 0 & 0 & 0 \\
0 & K_{P\_dr}^{inv}V_{od}^{inv} & 0 & 0 & 0 & 0 \\
-\dfrac{-V_{bd}^n\sin\delta_0^{inv}+V_{b,Q}^n\cos\delta_0^{inv}}{L_c} & -K_{P\_dr}^{inv}I_{oq}^{inv} & 0 & 0 & 0 & 0 \\
\dfrac{-V_{bd}^n\cos\delta_0^{inv}-V_{b,Q}^n\sin\delta_0^{inv}}{L_c} & K_{P\_dr}^{inv}I_{od}^{inv} & 0 & 0 & 0 & 0
\end{bmatrix}$$

$$A_{12}^{inv} = \begin{bmatrix}
0 & 0 & 0 & 0 & 0 & 0 & 0 & 0 \\
0 & 0 & 0 & 0 & \omega_c I_{od}^{inv} & \omega_c I_{oq}^{inv} & \omega_c V_{od}^{inv} & \omega_c v_{oq}^{inv} \\
0 & 0 & 0 & 0 & \omega_c I_{oq}^{inv} & -\omega_c I_{od}^{inv} & -\omega_c V_{oq}^{inv} & \omega_c V_{od}^{inv} \\
0 & 0 & 0 & 0 & 0 & 0 & 0 & 0 \\
0 & 0 & 0 & 0 & -1 & 0 & 0 & 0 \\
0 & 0 & 0 & 0 & 0 & -1 & 0 & 0 \\
0 & 0 & -1 & 0 & -K_{pv} & -\omega_0 C_f & F & 0 \\
\dfrac{K_{ii}}{L_f} & 0 & 0 & -1 & \omega_0 C_f & -K_{pv} & 0 & F \\
-\dfrac{R_f+K_{pi}}{L_f} & \omega_{sys}-\omega_0 & \dfrac{1+K_{pv}\,K_{pi}}{L_f} & \dfrac{-\omega_0 C_f\,K_{pi}}{L_f} & \dfrac{F\,K_{pi}}{L_f} & 0 & \dfrac{1}{L_c} & 0 \\
0 & \dfrac{K_{ii}}{L_f} & -\omega_{sys}+\omega_0 & -\dfrac{R_f+K_{pi}}{L_f} & \dfrac{\omega_0 C_f\,K_{pi}}{L_f} & -\dfrac{1+K_{pv}\,K_{pi}}{L_f} & 0 & \dfrac{F K_{pi}}{L_f} \\
0 & 0 & \dfrac{1}{C_f} & 0 & 0 & -\omega_{sys} & -\dfrac{1}{C_f} & 0 \\
0 & 0 & 0 & \dfrac{1}{C_f} & -\omega_{sys} & 0 & 0 & -\dfrac{1}{C_f} \\
0 & 0 & 0 & 0 & \dfrac{1}{L_c} & 0 & -\dfrac{R_c}{L_c} & \omega_{sys} \\
0 & 0 & 0 & 0 & 0 & \dfrac{1}{L_c} & -\omega_{sys} & -\dfrac{R_c}{L_c}
\end{bmatrix}$$

$$B_{Q,i}^g = [b(j,k)_{Q,i}^g]_{14\times14} \tag{A.31}$$

$$b_{Q,i=g}^g(j,k) = \begin{cases} \alpha_Q^g - 1, & if\ j = 4\ and\ k = 3 \\ 0, otherwise \end{cases} \tag{A.32}$$

$$b_{Q,i\neq g}^{(g)}(j,k) = \begin{cases} \alpha_Q^g, & if\ j = 4\ and\ k = 3 \\ 0, otherwise \end{cases} \tag{A.33}$$

$$b(j,k)^{(g)}_{P,i=g} = \begin{cases} K^g_{P\_sh}\alpha^g_P - K^g_{P\_sh}, & if\ j = 1, k = 2 \\ I^g_{iq}\left[K^g_{P\_sh}\alpha^g_P - K^g_{P\_sh}\right], & if\ j = 9, k = 2 \\ -I^g_{id}\left[K^g_{P_{sh}}\alpha^g_P - K^g_{P_{sh}}\right], & if\ j = 10, k = 2 \\ V^g_{oq}\left[K^g_{P_{sh}}\alpha^g_P - K^g_{P_{sh}}\right], & if\ j = 11, k = 2 \\ -V^g_{od}\left[K^g_{P_{sh}}\alpha^g_P - K^g_{P_{sh}}\right], & if\ j = 12, k = 2 \\ I^g_{oq}\left[K^g_{P_{sh}}\alpha^g_P - K^g_{P_{sh}}\right], & if\ j = 13, k = 3 \\ -I^g_{od}\left[K^g_{P_{sh}}\alpha^g_P - K^g_{P_{sh}}\right], & if\ j = 14, k = 2 \\ 0, & otherwise \end{cases}$$

$$b(j,k)^g_{P,i\neq inv} = \begin{cases} K^g_{P\_sh}\alpha^g_P, & if j = 1, k = 2 \\ I^g_{iq}K^g_{P\_sh}\alpha^g_P, & if\ j = 9, k = 2 \\ -I^g_{id}K^g_{P\_sh}\alpha^g_P, & if\ j = 10, k = 2 \\ V^g_{oq}K^g_{P\_sh}\alpha^g_P, & if\ j = 11, k = 2 \\ -V^g_{od}K^g_{P\_sh}\alpha^g_P, & if\ j = 12, k = 2 \\ I^g_{oq}K^g_{P\_sh}\alpha^g_P, & if\ j = 13, k = 2 \\ -I^g_{od}K^g_{P\_sh}\alpha^g_P, & if\ j = 14, k = 2 \\ 0, & otherwise \end{cases}$$